



# Thermal oxidation of carbon in organic matter rich volcanic soils: insights into SOC age differentiation and mineral stabilization

Katherine E. Grant · Valier V. Galy · Oliver A. Chadwick · Louis A. Derry

Received: 21 August 2018 / Accepted: 6 August 2019  
© Springer Nature Switzerland AG 2019

**Abstract** Radiocarbon ages and thermal stability measurements can be used to estimate the stability of soil organic carbon (OC). Soil OC is a complex reservoir that contains a range of compounds with different sources, reactivities, and residence times. This heterogeneity can shift bulk radiocarbon values and impact assessment of OC stability and turnover in soils. Four soil horizons (Oa, Bhs, Bs, Bg) were sampled from highly weathered 350 ka Pololu basaltic volcanics on the Island of Hawaii and analyzed by Ramped PyrOX (RPO) in both the pyrolysis (PY) and oxidation (OX) modes to separate a complex mixture of OC into thermally defined fractions. Fractions were

characterized for carbon stable isotope and radiocarbon composition. PY and OX modes yielded similar results. Bulk radiocarbon measurements were modern in the Oa horizon ( $Fm = 1.013$ ) and got progressively older with depth: the Bg horizon had an  $Fm$  value of 0.73. Activation energy distributions ( $p(E)$ ) calculated using the ‘rampedpyrox’ model yielded consistent mean  $E$  values of  $140 \text{ kJ mol}^{-1}$  below the Oa horizon. The ‘rampedpyrox’ model outputs showed a mostly bimodal distribution in the  $p(E)$  below the Oa, with a primary peak at  $135 \text{ kJ mol}^{-1}$  and a secondary peak at  $148 \text{ kJ mol}^{-1}$ , while the Oa was dominated by a single, higher  $E$  peak at  $157 \text{ kJ mol}^{-1}$ . We suggest that mineral-carbon interaction, either through mineral surface-OC or metal-OC interactions, is the stabilization mechanism contributing to the observed mean  $E$  of  $140 \text{ kJ mol}^{-1}$  below the Oa horizon. In the Oa horizon, within individual RPO analyses, radiocarbon ages in the individual thermal fractions were indistinguishable ( $p > 0.1$ ). The flat age distributions indicate there is no relationship between age and thermal stability ( $E$ ) in the upper horizon ( $> 25 \text{ cm}$ ). Deeper in the soil profile higher  $\mu E_f$  values were associated with older radiocarbon ages, with slopes progressively steepening with depth. In the deepest (Bg) horizon, there was the largest, yet modest change in  $Fm$  of 0.06 (626 radiocarbon years), indicating that older OC is slightly more thermally stable.

Responsible Editor: Marc G. Kramer.

**Electronic supplementary material** The online version of this article (<https://doi.org/10.1007/s10533-019-00586-1>) contains supplementary material, which is available to authorized users.

K. E. Grant (✉) · L. A. Derry  
Department of Earth and Atmospheric Sciences, Cornell University, 112 Hollister Drive, Ithaca, NY 14853, USA  
e-mail: keg89@cornell.edu

V. V. Galy  
Department of Marine Chemistry and Geochemistry,  
Woods Hole Oceanographic Institution, 266 Woods Hole Road, Woods Hole, MA 02543, USA

O. A. Chadwick  
Department of Geography, University of California, Santa Barbara, Oakland, CA 93106, USA

**Keywords** Soil organic carbon (SOC) · Ramped pyrolysis/oxidation (RPO) · Radiocarbon

## Introduction

Soil organic carbon (SOC) is the largest terrestrial reservoir of organic carbon (C), holding an estimated 2800 Pg C in the upper 3 m of soil globally (Jackson et al. 2017). It is heterogeneous in chemistry, morphology, and reactivity. Its long-term stability as a net C sink is uncertain, especially under changing environmental conditions (Bradford et al. 2016; Davidson and Janssens 2006). A common model to determine SOC stability depicts distinct carbon pools with variable turnover times, as measured by a radiocarbon ( $^{14}\text{C}$ ) age (Trumbore 2009). In tropical volcanic soils, SOC with old radiocarbon ages is associated with mineral soil (Torn et al. 1997), but it can co-exist with modern plant-derived material transported downwards via macropore flow, leading to a heterogeneous age mixture of carbon compounds within individual soil horizons (Marin-Spiotta et al. 2011). The introduction of modern carbon down the soil profile can significantly shift the bulk radiocarbon ages to younger values and could introduce bias when using  $^{14}\text{C}$  to calculate turnover time and C reservoir stability. Along with the mixture in  $^{14}\text{C}$  ages at depth, there is a mixture of OC with different reactivities because OC stability is a function of OC compound structure and its interaction with mineral surfaces, bridging cations, and other organic compounds (Lehmann and Kleber 2015; Schmidt et al. 2011). Consequently, bulk  $^{14}\text{C}$  measurements may not adequately describe the soil system in which SOC consists of a wide range of components with various reactivities and ages in a single sample.

To address the need for a greater understanding of SOC reactivity and  $^{14}\text{C}$  age distribution in soils we investigate the use of the newly developed Ramped PyrOx accelerator mass spectrometry technique (thereafter referred to as RPO) that can elucidate the age and reactivity distributions of SOC in a single sample. We ask how the  $^{14}\text{C}$  “age” in a single soil sample, representing a complex mixture, can be interrogated using the RPO technique which provides a  $\text{CO}_2$ -weighted age distribution along with a distribution of activation energies (Hemingway et al.

2017b; Rosenheim et al. 2008). Techniques measuring thermal reactivity have been widely used to assess soil organic matter stability, but few studies have directly measured carbon isotopic measurements and thermal reactivity (Lopez-Capel et al. 2008; Plante et al. 2009). By combining thermal activation energy analysis with environmental tracers such as radiocarbon and stable isotopes, we can directly probe the relationship between SOC reactivity, source, and age.

The coupling of RPO and AMS  $^{14}\text{C}$  measurements is relatively recent, and most work to date has been carried out in riverine and aquatic sedimentary systems to understand the age spectrum and source variation of OC deposited in these environments (Bianchi et al. 2015; Rosenheim and Galy 2012; Schreiner et al. 2014; Williams and Rosenheim 2015). One study applied RPO- $^{14}\text{C}$  in oxidation (OX) mode to an active soil system (Plante et al. 2013), and recently the pyrolysis (PY) approach was used to examine carbon sources in a paleosol (Vetter et al. 2017). RPO analysis of sediments and soils demonstrate that these sinks store OC with a wide range of properties. RPO analyses have been used to measure sedimentary depositional systems, successfully separating OC with distinct sources having large differences in age ( $> 20,000$   $^{14}\text{C}$  yrs) and reactivities ( $100 \text{ kJ mol}^{-1}$  to  $> 200 \text{ kJ mol}^{-1}$ ) within a single sample. Sediments, either due to environmental differences or source contributions, can have a wide range of  $^{14}\text{C}$  content (expressed as fraction modern—*Fm*) among fractions of increasing thermal recalcitrance, while existing data on soils run with the same techniques show much smaller differences in *Fm* values among thermal fractions (Vetter et al. 2017; Plante et al. 2013). Sediments also tend to have broad and complex distributions of activation energy, while soils generally have simpler and narrower distributions (Hemingway et al. 2019). Zhang et al. (2017) used RPO analyses to identify sources of carbon in sediments derived from permafrost erosion, but did not specifically consider the energetics. Hemingway et al. (2018) attributed large *Fm* differences in soil thermal fractions to rapidly eroding bedrock and soil formation in Taiwanese landscapes via the mixing of  $^{14}\text{C}$ -dead petrogenic OC and young biogenic OC within the soil profile. A study of paleosols using RPO showed invariant ages between thermal fractions which was attributed to paleosol burial and isolation from the environment, rather than a property of the soil

prior to burial (Vetter et al. 2017). Yet, it remains unclear why RPO analysis of sediments and soils show differences: is it a method artifact or does it reveal a fundamental difference between carbon in soils and sediments?

Here we apply the coupled RPO- $^{14}\text{C}$  approach to a tropical volcanic soil in order to test the method's applicability to a dynamic soil system with a range of  $^{14}\text{C}$  inputs. In this pilot scale study, we test whether RPO can distinguish changing chemical signals between soil horizons. We use Pu'u Eke, a well-studied SOC-rich site on Kohala Mountain, Hawaii to test the RPO system on modern, active soils (Kramer et al. 2012; Marín-Spiotta et al. 2014). Nearby and closely related soils in Hawaii are known for "old" SOC ages estimated from  $^{14}\text{C}$  activity, in some cases over 10,000  $^{14}\text{C}$  years (Torn et al. 1997). The Pu'u Eke soil has a combination of carbon from distinct sources: macropore DOC, mineral bound OC and microbially degraded OC. We expect the three sources to have different  $^{14}\text{C}$  ages and thermal properties. Thus Pu'u Eke soils should provide a useful test of whether isotope-enabled RPO techniques can enhance our understanding of carbon turnover in chemically complex soil environments. We seek to gain additional insight into the age distribution and reactivity of the large stores of organic carbon stored in volcanic soils.

## Materials and methods

### Site/sample description

Soil samples were collected in April 2013 from the Pu'u Eke (20°4'42"N, 155°43'44"W) site on the leeward side of Kohala volcano, on the Island of Hawai'i. The Pu'u Eke soil sits at 1500 m and is underlain by 350 ka Pololu lava flow and supports an O'hia (*Metrosideros polymorpha*) and Hapu'u pulu (tree fern: *Cibotium splendens*) forest. All vegetation near the site uses the C3 photosynthetic pathway. The site receives about 2800 to 3500 mm of rainfall per year (Giambelluca et al. 2013, 1986), though rain gauges are not in place at the site and precipitation is spatially variable, so precipitation remains uncertain and may well be higher. Soils are categorized as Hydric Hapludand or Hydric Placudand (Kramer et al. 2012; Marín-Spiotta et al. 2011). Soil pits were dug to ~ 1 m and sampled for genetic horizon using

standard methods detailed in Kramer et al. (2012). Horizons were designated as follows: the Oa is a subsurface horizon with strong organic accumulation, Bhs contains both organic and Fe accumulations, the Bs shows significant Fe and Al accumulation, and the Bg has Fe loss due to anoxia induced reduction processes (SI Table S1). Samples were sent to Cornell University and stored field moist at 4 °C until analysis. In the laboratory, field moist samples were homogenized, sieved to < 2 mm and freeze dried. Excess sample was stored at 4 °C.

The Pu'u Eke soil and other soils on Kohala have similar properties and have been extensively studied to understand the relationships among edaphic properties and soil carbon sequestration (Buettner et al. 2014; Chadwick et al. 2003, 2007; Kramer et al. 2012; Marín-Spiotta et al. 2011; Torn et al. 1997). Marín-Spiotta (2011) presented a detailed assessment of Pu'u Eke soils, where mineral matrix OC is distinct from macropore OC. The re-allocation of modern OC to belowground horizons was facilitated by DOC flow down large crack structures. Data presented in Marín-Spiotta (2011) shows shifts in the C/N ratio, NMR spectra, and radiocarbon ages, depicting a range of age and OC degradation in the mineral horizons.

The soils are composed of a mineral matrix of Al-oxy/hydroxides allophane and imogolite with nano-mineral and colloidal Fe phases, such as nano-goethite (Marín-Spiotta et al. 2011; Thompson et al. 2006b). Occasional periods of saturation create an active redox environment that stimulates formation of mineral-bound carbon assemblages, especially those involving Fe oxides (Thompson et al. 2006a, b). This frequent variation in soil saturation, redox state, and increased organic acid input in the upper horizons causes the pH values to range from 3.7 in the Oa to 4.5 in the Bs and Bg horizons (Marín-Spiotta et al. 2011), where Fe reduction causes an increase in pH values in the deeper, anoxic environment. Mineral dust supplies the near-surface horizons with some SiO<sub>2</sub> and base cations (Kurtz et al. 2001).

We selected these soil samples for RPO measurement because previous work has shown these samples contain a mixture of macropore OC originating in surface horizons and soil carbon closely associated with the mineral matrix, which have distinct  $^{14}\text{C}$  signatures. Each soil horizon was sampled volumetrically, specifically not separating interior matrix carbon from macropore carbon to test if RPO can

successfully resolve signals from these two distinct sources. The soils are well-suited for RPO measurement because they formed from one parent material, the Pololu lava flow (350 ka), they receive relatively simple plant inputs, and contain no sedimentary, petrogenic C ( $^{14}\text{C}$ -dead). Four soil samples (Table 1) were obtained from a single pit, sampled in coordination with a larger sampling campaign.

## Geochemistry

Inorganic elemental analysis was done at Cornell University and compared to previous measurements presented in the literature and to unpublished data (O. Chadwick). Samples were dried at 105 °C for 24 h prior to pulverization with an agate shatter box. Samples were combusted in a muffle furnace at 500 °C for 4 h and then ignited at 950 °C for 30 min to remove all OC and structural water and convert  $\text{Fe}^{2+}$  to  $\text{Fe}^{3+}$ . Total metal analyses were carried out by microwave digestion with  $\text{HNO}_3/\text{HCl}/\text{HF}$  using an Ethos Milestone Microwave Digester (Milestone Scientific, Inc., Livingston, NJ). Ignited samples were digested in a 3:2:0.25 solution of  $\text{HNO}_3/\text{HCl}/\text{HF}$  at 200 °C for 40 min. Samples were cooled to 25 °C and 4 wt% boric acid was added; the solution was reheated to 150 °C for 20 min to neutralize excess HF, while retaining dissolved  $\text{SiO}_2$ . The USGS standard BHVO-2 was used as a reference material and procedural blanks measured every 10 samples. Upon digestion, samples were immediately diluted to 10,000  $\times$  for analysis on the SpectroBlue ICP-OES (Ametek, Kleve, Germany) for major elements and 20,000  $\times$  for trace metal analysis on the Thermo Element II ICP-MS (Thermo Fisher Scientific, Waltham, MA). Quantification was achieved using matrix matched intensity calibration curves for both the ICP-OES and ICP-MS runs. Analytical uncertainties are within 5%, based on repeat analysis of standards and

of selected samples. Element loss or gains are calculated relative to an “immobile” element ( $i$ ), in this case, niobium (Nb), and normalized to the unweathered parent material ( $p$ ) (Kurtz et al. 2000). The mass transfer coefficients,  $\tau_{ij}$ , (1) are a measure of weathering where the abundance of a mobile element ( $j$ ) in the weathered material ( $w$ ) is compared to an immobile element ( $i$ ).

$$\tau_{ij} = \left( \frac{C_{i,p}}{C_{i,w}} \times \frac{C_{j,w}}{C_{j,p}} \right) - 1 \quad (1)$$

Bulk samples were dried in a 60 °C oven, homogenized by lightly grinding with a mortar and pestle, and loaded into tin capsules for combustion. Total organic carbon (TOC), nitrogen (TN),  $\delta^{13}\text{C}$ , and  $\delta^{15}\text{N}$  were measured at the Cornell Stable Isotope Laboratory on a Thermo Delta V Advantage coupled EA-IRMS (Thermo Scientific, Waltham, MA, USA). Data were corrected following standard procedures;  $\delta^{13}\text{C}$  is reported relative to Vienna Pee Dee Belemnite (VPDB) and  $\delta^{15}\text{N}$  is reported relative to the  $^{15}\text{N}/^{14}\text{N}$  ratio in air.

## Ramped pyrolysis/oxidation (RPO)

Ramped temperature pyrolysis/oxidation (RPO) analysis was carried out at the National Ocean science accelerator mass spectrometer facility at woods hole oceanographic Institution. Four samples were measured in both oxidation (OX) and pyrolysis (PY) configurations. The RPO technique and instrumental set up is detailed in Rosenheim et al. (2008) and Hemingway et al. (2017a). Briefly, all glassware is combusted at 850 °C for quartz and 450 °C for Pyrex. Depending on %OC, 20–60 mg of freeze-dried, homogenized soil is loaded between quartz wool into a quartz reactor insert. The reactor is placed into the top of a dual oven, ramped at 5 °C/min, while the bottom oven was held constant at 800 °C. The sample

**Table 1** Characterization table for Pu’u Eke soils in this study

Sample designation	Depth (cm)	Horizon	%OC	$\delta^{13}\text{C}$	$\delta^{15}\text{N}$	Age ( $^{14}\text{C}$ years)	Age (Fm)
PE-1	13–21	Oa	49.2 $\pm$ 0.2	– 26.16	3.72	Modern	1.01
PE-2	25–36	Bhs	17.00 $\pm$ 1.18	– 26.21	2.55	1028	0.88
PE-3	40–55	Bs	12.74 $\pm$ 0.09	– 26.58	2.33	1937	0.79
PE-4	63–74	Bg	9.86 $\pm$ 0.10	– 26.47	0.57	2528	0.73

is heated under an atmosphere of He (ultrapure) for PY or 92% He:8%O<sub>2</sub> for OX with a 32 mL/min flow rate. Evolved gases are passed through the bottom oven where an additional 3 mL/min of O<sub>2</sub> (PY) or 92:8 He:O<sub>2</sub> (OX) is added and gas is passed over a Cu, Pt, and Ni catalyst wire to ensure complete conversion to CO<sub>2</sub> in both configurations. Evolved CO<sub>2</sub> flows through a water trap (dry ice and isopropyl alcohol) and is quantified using an infrared gas analyzer (IGRA) in parts per million by volume (ppmv CO<sub>2</sub>) with 1-second temporal resolution. CO<sub>2</sub> is collected in one of two liquid N<sub>2</sub> traps, which capture CO<sub>2</sub> at user defined intervals, referred to as ‘fractions’. Five fractions, referred to as F1–F5, were collected per sample. CO<sub>2</sub> was purified downstream on a vacuum line and flame-sealed in 6 mm Pyrex tubes containing ~ 100 mg CuO and ~ 10 mg Ag. Sealed samples were combusted at 525 °C to remove contaminant gases, graphitized, and measured for radiocarbon and δ<sup>13</sup>C following standard procedures (McNichol et al. 1994). All bulk and RPO fractions were measured for stable carbon isotope compositions using a dual-inlet isotope ratio mass spectrometer (IRMS) (McNichol et al. 1994). All radiocarbon data is presented as fraction modern notation (*Fm*) and is corrected for <sup>13</sup>C fractionation. RPO fraction masses, δ<sup>13</sup>C, and *Fm* are corrected for blank carbon contribution as described in Hemingway et al. (2017a). δ<sup>13</sup>C values are further corrected for kinetic fractionation as described in Hemingway et al. (2017a).

#### Activation energy analysis

RPO thermograms are analyzed using the open sourced ‘rampedpyrox’ Python package (Hemingway 2016) where the distributed activation energy model is solved inversely and yields a continuous distribution of activation energy (*E*) (Hemingway et al., 2017b). It makes no a priori assumptions about the distribution of activation energies, thereby resulting in a non-parametric activation energy distribution. The overall distribution as well as specific portions of it corresponding to RPO gas fractions can be characterized by their mean ( $\mu E$ ) and standard deviation ( $\sigma E$ ). In this case, the standard deviation refers to the variance of the distribution of *E* within the sample rather than an uncertainty in the measurement. It is a measure of the heterogeneity in the bonding environment within each sample. This approach permits the direct comparison

of the distribution of *E* in kJ mol<sup>-1</sup> within each RPO fraction to measured *Fm* and δ<sup>13</sup>C values in the same fraction (Hemingway et al. 2017b). Each thermogram is broken down into individually calculated  $\mu E_f$  and  $\sigma E_f$  values within each collected CO<sub>2</sub> fraction, *f*, where *f* = 1 to 5. It does not attempt to assign known, single component activation energies to these samples, rather it is an assessment of the overall chemical bonding environment of the organic matter. It is most effectively used to compare samples within an RPO data set, not necessarily to activation energies obtained by other methods. The *F<sup>14</sup>R* parameter (2), detailed in Soulet et al. (2016), which provides a time-insensitive metric of <sup>14</sup>C reservoir age, allows us to directly compare changes in the relationship between *Fm* values of the individual fractions and *E*.

$$F^{14}R_{x-y} = \frac{Fm_x}{Fm_y} \quad (2)$$

In this case, *x* indicates the individual thermal fractions (*f*<sub>1</sub>–*f*<sub>5</sub>) and *y* is designated as the youngest or most <sup>14</sup>C enriched fraction (*f*<sub>1</sub> in each sample).

## Results

### Geochemistry

This study uses one soil profile as an example of RPO methodology examined in the context of the previous studies to expand our understanding of the SOC in a highly weathered volcanic soil. Pu‘u Eke has highly weathered andic soils, with almost complete loss of major cations Na, Ca, Mg. Iron and Al are significantly lost in these soils with  $\tau_{Fe}$  values relative to Nb of < -0.6 for the profile, and  $\tau_{Al}$  of < -0.8 below 30 cm soil depth (Fig. 1).

The measured organic carbon content in the 13–21 cm horizon (Oa) is 49% and decreases to 9% in the deepest horizon (Table 1). The OC content is presented normalized to TiO<sub>2</sub> (Fig. 1) to show carbon addition to the soil profile in relation to other mass losses or gains. Other studies of Pu‘u Eke soils show similar carbon storage values in the upper 1 m of soil, however, our horizons contain more carbon on average than most of the other sampled soil pits at this site. This may be due to soil heterogeneity; in particular we think our soil pit contained more organic infillings as

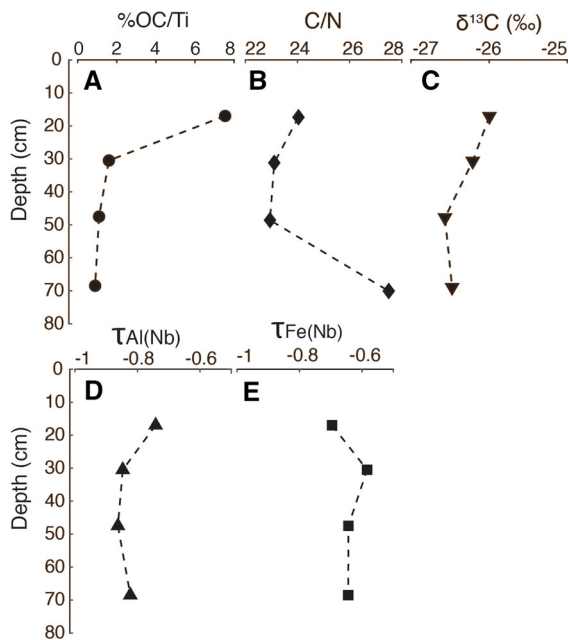


**Fig. 1** Panel A–E depict a subset of the geochemical analysis done on these soils. **A** normalized carbon content shows a decline of C in the system. The normalized parameter shows carbon addition to the system relative to the initial soil mass. **B** the C/N ratio is relatively stable around  $\sim 23$  until a sharp increase below the Bs horizon (50 cm). **C** Stable isotope data ( $\delta^{13}\text{C}$ ) shows there is only C3 input into the soil system. There is a slight enrichment of shallower horizons. **D** Al is subject to substantial weathering losses. **E** Fe loss is also extensive, and is greatest in the shallower horizons

described in (Marin-Spiotta et al. 2011). The bulk  $\delta^{13}\text{C}$  values range from  $-26.0\text{‰}$  in the top 13–21 cm Oa horizon to  $-26.6\text{‰}$  at depth 63–74 cm Bg horizon (Fig. 1). The relatively constant bulk  $\delta^{13}\text{C}$  confirms a uniform C3 plant input from the upper horizons. In other soil pits at Pu‘u Eke, bulk  $\delta^{13}\text{C}$  increased from  $-29$  or  $-30\text{‰}$  in shallow horizons to  $-26.5\text{‰}$  at depth, yet the organic infillings show a similar pattern to our bulk measurements (Marin-Spiotta et al. 2011). The C:N ratio is similar to that reported in previously published work at this site, with C:N ratios increasing with depth from 24.0 to 27.5, indicating either a preferential decomposition of nitrogen-containing species or the accumulation of plant-derived compounds as was proposed in Kramer et al. (2012), or some combination of the two.

Bulk radiocarbon (Table 1) shows a systematic decrease from a modern  $Fm$  value of 1.013 in the Oa horizon to 0.730 ( $\Delta^{14}\text{C} = -265\text{‰}$ ) in the Bg horizon. In our soils, the bulk radiocarbon data in the upper

three horizons are similar to the bulk measurements from other studies (SI Fig. 1), but the Bg bulk radiocarbon measurement was younger than previously measured soils at Pu‘u Eke (Marin-Spiotta et al. 2011), where bulk  $^{14}\text{C}$  measurements in the Bg horizon were  $-600\text{‰}$ . Our data are consistent with the presence of organic infillings associated with younger radiocarbon values, indicating a greater input of young carbon at depth. This highlights the large heterogeneity of these systems as well as the ability of young carbon to contribute to the SOC at depth ( $> 70$  cm).

### Ramped pyrolysis/oxidation (RPO)

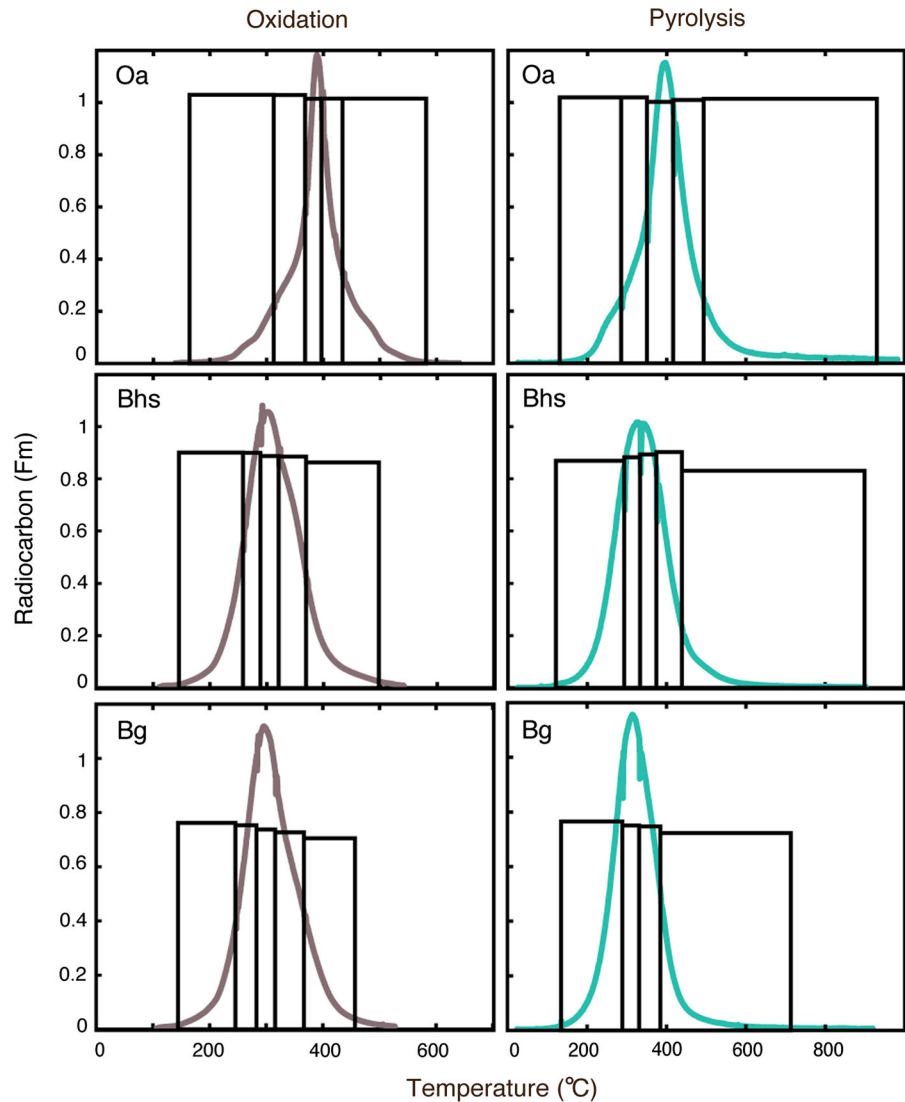
Radiocarbon activity was determined on five  $\text{CO}_2$  fractions ( $f_1$ – $f_5$ ) released at increasing temperatures from each RPO run (SI Table S2). For the individual RPO experiments on the Oa, Bhs, and Bg horizons in both the OX and PY modes, the  $Fm$  values of  $f_1$ – $f_5$  are statistically the same ( $p > 0.4$ ) (Fig. 2), with the mass weighted average of  $f_1$ – $f_5$  equaling the measured bulk value. In OX mode, there is a small but significant systematic decrease in  $Fm$  from  $f_1$  to  $f_5$  in both the Bhs (from 0.89 to 0.85) and the Bg horizon (0.76 to 0.71). The RPO normalized thermograms (Fig. 3) in OX and PY modes show minimal variability in peak shape and  $T$ -max for the samples below 25 cm depth. There is a small difference in the  $T$ -max from the Bhs and Bg in the PY mode, which we believe to be an experimental artifact attributed to reactor variability and  $\text{O}_2$  back flow. This variability does not appear in the OX experiments. We conclude there is no discernable systematic difference in the  $Fm$  distributions obtained in the PY and OX modes.

Measured stable carbon isotopes of fractions showed no trend within a single RPO run (SI Table 1).  $\delta^{13}\text{C}$  values varied by  $\leq 1.7\text{‰}$  across the fractions within a given horizon (e.g. Bhs), and there is no resolvable difference between fraction data obtained in the PY and OX modes.

### Activation energy model

The distribution of  $E$  for each horizon in the OX and PY mode are presented in Fig. 4. In the OX experiments, the shallow Oa horizon had a  $\mu E$  of  $159.2 \text{ kJ mol}^{-1}$  and a dominant peak at  $157.9 \text{ kJ mol}^{-1}$  (Fig. 4). This horizon also had the

**Fig. 2** Comparison of thermograms from the OX (left side) and PY (right side) experiments. The panels are arranged in order from the Oa (13–21 cm) horizon on top to the Bg (63–74 cm) horizon on the bottom. The normalized evolved CO<sub>2</sub> (unitless) is the thick green line, while the histograms indicate *Fm* values of each fraction measured for radiocarbon in the experiment. Analytical errors are not represented on the graph as they are smaller than the histogram line thickness. Differences in *Fm* between fractions in an individual experiment are small, and the *Fm* values average to bulk values within a single experiment



largest  $\sigma E$  of the OX experiments. The  $\mu E$  values were constant below the Oa horizon, with values close to  $140 \text{ kJ mol}^{-1}$ , and  $\sigma E$  showed no systematic variations in the  $11.5\text{--}13.1 \text{ kJ mol}^{-1}$  range (Table 2, Fig. 5), suggesting the bonding environment is similar. Below the Oa horizon, the mineral horizons'  $E$  distributions show a primary peak at  $\sim 135 \text{ kJ mol}^{-1}$  and a second, smaller peak at  $\sim 147 \text{ kJ mol}^{-1}$ . This secondary peak is more prominent in the Bhs horizon than deeper in the soil. In the PY experiments, the model outputs have 'broader' peaks, with the Oa and Bg consistent with the OX experiments, but the Bhs shows a less distinctive bimodal distribution. The activation energy

distributions for the fractions obtained in PY mode also have larger standard deviations ranging from  $\sigma E = 20.9 \text{ kJ mol}^{-1}$  for the Oa to  $15.7 \text{ kJ mol}^{-1}$  for the Bg (Table 1). The  $\mu E$  of the Oa is significantly different than the  $\mu E$  of the three mineral horizons ( $p < 0.026$ ).

Additionally, the  $\mu E_f$  energies ranged from  $123$  to  $204 \text{ kJ mol}^{-1}$  (SI Table 2) depending on the sample. In Fig. 6, we show for each horizon both the unnormalized  $F_m$  values and the  $F^{14}R$  values compared to the mean  $E$  value of each fraction, where the unnormalized slope for the Oa horizon is nearly flat ( $-0.0005$  and  $r^2$  of  $0.63$ ), but the slope becomes progressively negative with depth, from  $-0.0011$  to

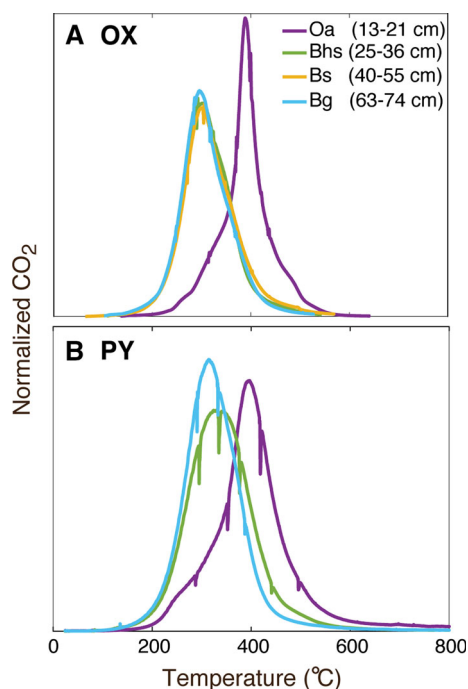


**Fig. 3** Panel A depicts RPO runs in oxidation mode, where  $T_{max}$  is shifted towards lower temperatures deeper in the soil profile and the Oa horizon (organic rich) is shifted towards higher temperatures. In this mode, there is no difference in  $T_{max}$  or thermogram shape below the Bhs horizon. Panel B shows the pyrolysis mode runs for the same set of samples. Thermograms have relatively similar shapes, with a unimodal peak distribution

– 0.0017 ( $r^2$  of 0.93 and 0.98 respectively) from the Bhs to the Bg. We found negative correlations between  $E$  and  $Fm$  in all three measured OX horizons, however only the Bhs and Bg were statically significant with  $p < 0.05$  (Fig. 6). This change with depth is more clearly represented using  $F^{14}R$  where the change in the slope of Bhs to Bg is from  $-0.0014$  to  $-0.0022$  ( $r^2$  of 0.93 and 0.98). In the Oa, there was minimal correlation ( $r^2 = 0.63$ ,  $p > 0.1$ ) between  $Fm$  and  $E$  or  $\delta^{13}C$ . In deeper horizons older OC has higher  $E$ . The correlation was present in both PY and OX modes.

## Discussion

### RPO PY and OX are indistinguishable

While there are theoretical and methodological differences between the two instrument modes PY and OX, there is overall good agreement between data

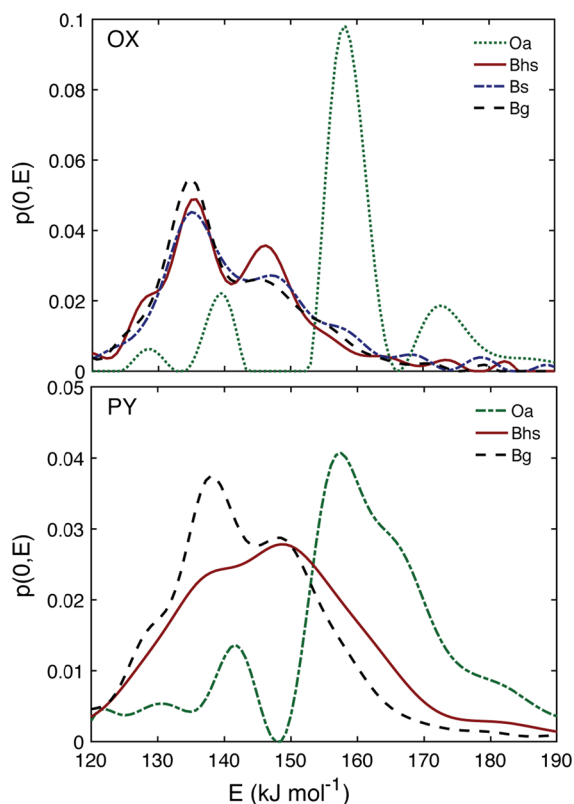


**Fig. 4** ‘rampedpyrox’ Model outputs from the four Pu‘u Eke soil horizons in the OX (upper panel) and PY (lower panel). All model experiments were run with the same parameters and outputs are mass normalized distributions. The Oa has a shifted  $p(E)$  towards higher activation energies. In the OX experiments, the Bhs has a bimodal distribution, with a dominate peak at  $135 \text{ kJ mol}^{-1}$  and a second peak at  $\sim 146 \text{ kJ mol}^{-1}$ . The amplitude of this peak is progressively reduced in the two deeper horizons. In the PY output, the bimodal distribution is apparent, yet with less definition in the Bhs

obtained in PY and OX modes (Fig. 1, Fig. 3, SI Table S2). We find however that the activation energy distributions obtained from OX mode runs are characterized by smaller  $\sigma E$  than in the PY mode, perhaps reflecting more prominent charring effects in the latter (Williams et al. 2014). The model was optimized for the OX mode, yet it theoretically can be used in any time–temperature regime to analyze thermal decomposition curves as long as decomposition occurs following first order kinetics (Hemingway et al. 2017b). The OX mode avoids some potential experimental artifacts which may be produced in pyrolysis experiments. This can occur during PY experiments when lower temperature products are converted to more thermally stable chemicals, which themselves

**Table 2** Thermal activation energy data calculated by the ‘rampedpyrox’ python package

Sample designation	Depth (cm)	Horizon	T-max OX (°C)	T-max PY (°C)	OX $\mu E$ (kJ/mol)	OX $\sigma E$ (kJ/mol)	PY $\mu E$ (kJ/mol)	PY $\sigma E$ (kJ/mol)
PE-1	13–21	Oa	389	395	159.13	12.41	163.21	20.90
PE-2	25–36	Bhs	300	333	140.63	11.91	148.02	17.46
PE-3	40–55	Bs	301	n.m.	141.98	13.11	n.m. <sup>a</sup>	n.m. <sup>a</sup>
PE-4	63–74	Bg	296	313	139.71	11.54	144.01	15.74

<sup>a</sup>PE-3 was not measured in pyrolysis mode

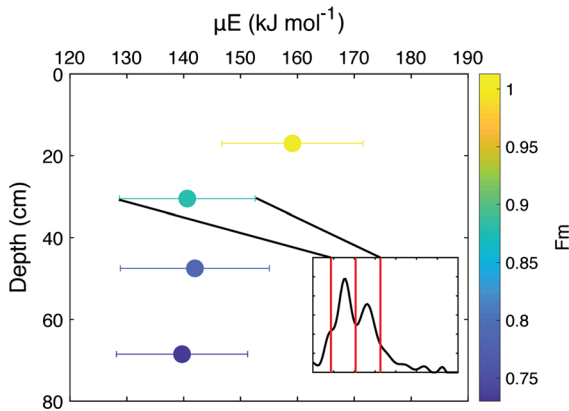


**Fig. 5** Depth profile of RPO  $\mu E$  for Pu'u Eke samples. Samples below 30 cm are identical in both the PY and OX modes for thermal activation energy. Activation energies in the Oa horizon are higher than deeper samples, implying both increased temperature sensitivity and higher thermal stability. Bulk  $F_m$  values show decreases down the profile while the  $\mu E$  shows no change. Plot insert: ‘rampedpyrox’ model output ( $p(E)$ ) for the Bhs is shown in the black line, while  $\mu E$  and  $\sigma E$  are shown in the red lines. This model output is the distribution of activation energies and can be represented as a mean and standard deviation

are decomposed at higher temperatures (so-called charring), leading to skewed thermograms (Williams et al. 2014). However, such byproducts typically appear at higher  $T$  ( $> 600$  °C). We observed no residual C evolved past 600 °C in any experiment. Also, the PY mode has, in some instances, permitted  $O_2$  flow back into the reactor resulting in partial oxidation instead of pure pyrolysis. For future experiments in soils, we thus recommend the OX mode as the most reliable. In the case of Pu'u Eke soils, the PY and OX modes on the RPO instrumentation can however be used interchangeably, and our overall results are independent of the method used.

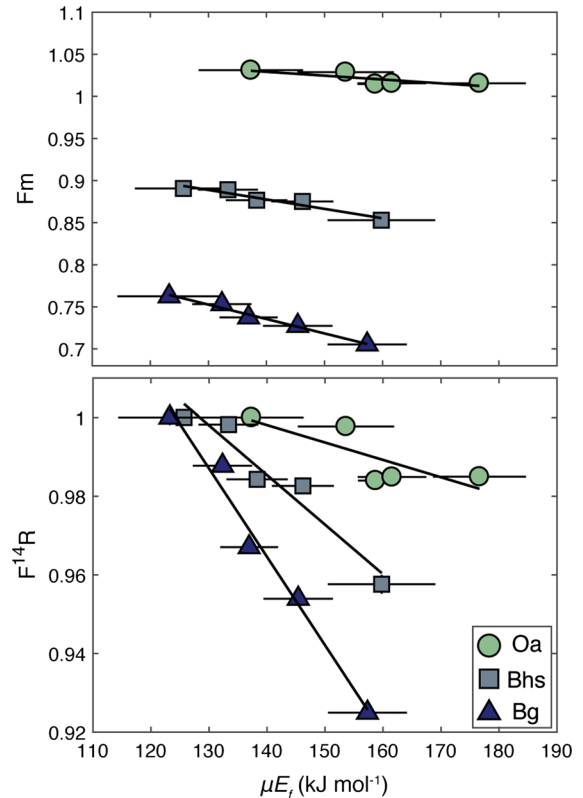


**Fig. 6** **Upper Panel:** Pu'u Eke Oa, Bhs Bg RPO run in OX mode where thermograms are analyzed with the ‘rampedpyrox’ python package. Model output directly relates  $\mu E_f$  and  $F_m$  of each individually collected fractions; slope and  $r^2$  for Oa are  $-0.0005$  and  $0.63$ , Bhs  $-0.0011$  and  $0.93$ , Bg  $-0.0017$  and  $0.981$  respectively. Error bars on the  $x$ -axis indicate the  $\sigma E$  of the distribution of  $E$  within each fraction, while vertical error bars represent the analytical error in  $F_m$ . For the Bg horizon, the absolute change in  $F_m$  is small, less than  $0.06$ , which corresponds to 626 radiocarbon years. **Lower Panel:** Comparison of the  $F^{14}R$  metric and  $\mu E_f$ . Data is normalized to the most  $^{14}C$ -rich (i.e. youngest) fraction for clearer comparison between samples of contrasted bulk  $^{14}C$  ages. Slope and  $r^2$  for Oa are  $-0.0004$  and  $0.63$ ; Bhs  $-0.0013$  and  $0.93$ ; Bg  $-0.0022$  and  $0.98$  respectively

## Stable $\mu E$ indicates single C stabilization mechanism in deep mineral horizons

The development of the ‘rampedpyrox’ program for RPO has increased our understanding of the thermochemical stability of OC (Hemingway et al. 2017b). The RPO instrument in soils is seen as an in situ experiment as no chemical pretreatment or separations are performed. In the three deeper horizons (Bhs, Bs and Bg) the  $\mu E$  values are essentially constant near  $140 \text{ kJ mol}^{-1}$  (Fig. 5). In the upper-most Oa horizon, the  $\mu E$  ( $159 \text{ kJ mol}^{-1}$ ) is about  $25 \text{ kJ mol}^{-1}$  higher, implying greater thermal stability. The OC in the Oa horizon is both much more abundant (49 wt%) and has different chemistry than the deeper horizons. Previous studies find a higher proportion of microbially-derived compounds in the Oa compared to deeper horizons, which contain more oxidized lignin (Kramer et al. 2012). Although we do not have thermograms of Pu’u Eke DOC, thermograms of the Oa horizon OC closely resemble samples of river DOC previously run on the RPO instrument (Hemingway et al. 2019), where the distributions of activation energy are characterized by relatively low  $\sigma E$  (10–15 kJ/mol) and  $\mu E$  values close to  $160 \text{ kJ/mol}$ . The similarity between Oa horizon and DOC thermograms is indicative of OC which has minimal mineral interactions, confirmed by the large OC/Ti in the Oa horizon (Fig. 1).

Below the Oa horizon,  $\mu E$  values were constant and lower ( $140 \text{ kJ mol}^{-1}$ ) in every sample regardless of increasing radiocarbon age. The activation energy model distributions (Fig. 4) are mostly bimodal, with maxima at  $135 \text{ kJ mol}^{-1}$  and at  $147 \text{ kJ mol}^{-1}$ . The deeper samples have substantially lower ratios of OC to mineral material, with OC/Ti ratio decreasing from 8 in the Oa horizon to  $< 2$  in the three deeper horizons (Fig. 1). The decrease in %OC and OC/Ti ratio suggests that there is relatively more mineral surface area available to interact with the OC below the Oa horizon. In the Oa horizon (OC content is 49 wt%), the amount of carbon suggests the mineral surfaces may be saturated leading to an abundance of OC not associated with the mineral matrix (Kaiser and Guggenberger 2003). In this case, the greater mean RPO  $E$  in the shallow Oa horizon likely reflects this mineral-unassociated organic material. From the Oa to the Bhs, there is a substantial decrease in the amount of OC from 49 to 17 wt% and an approximately four-fold decrease in OC/Ti. The substantially lower ratio of

carbon to mineral matrix implies a larger fraction of the OC is interacting with secondary aluminosilicates and metal hydroxides (e.g. Feng et al. 2013a, b; Ohno et al. 2017). The retained OC in the Bhs horizon and below contains more partially oxidized carbon than in the Oa horizon (Marin-Spiotta et al. 2011). This could lead to smaller, partially oxidized molecules at depth, which can be protected by interaction with the mineral matrix (Chorover et al. 2004; Kramer et al. 2012). These smaller molecules, most likely, are more thermally labile than the Oa material, as we see a shift from  $160 \text{ kJ mol}^{-1}$  in the Oa to  $140 \text{ kJ mol}^{-1}$  in deeper horizons. We hypothesize that mineral surface interactions would increase the  $\mu E$  and  $\sigma E$  of the activation energy distribution compared to unassociated, ‘left over’ material but not sufficiently to fully compensate for the decrease in  $\mu E$  associated with degradation processes that organic matter undergoes during early stage of soil formation. Overall, we therefore suggest that the decrease in  $\mu E$  between the Oa and deeper horizons reflects the transition from free un-associated organic material in the Oa horizon to mineral associated organic matter in the deeper horizons. In other settings, this framework is further supported by the higher mean thermal activation energy of light (free OM) than heavy (mineral associated OM) soil density fractions (Williams et al. 2018), and the differences in energy density of new versus persistent OM (Barre et al. 2016).

In the deeper Bhs, Bs and Bg horizons the differences in the distribution of RPO  $E$  also suggest changes in stabilization mechanisms, despite relatively small changes in the mean  $E$ . The amplitude of the peak at  $147 \text{ kJ mol}^{-1}$  in the  $p(0,E)$  values decreases with depth while the amplitude of the peak at  $135 \text{ kJ mol}^{-1}$  increases slightly. We hypothesize that the higher energy peak likely represents a chemically distinct pool of OC, while the lower  $E$  ( $135 \text{ kJ mol}^{-1}$ ) peak represents mineral-stabilized C. However, these differences in the model output represent small changes compared to the sample thermograms which are very similar.

Interaction with mineral surfaces is thought to be a driver of SOC stability in volcanic soils (Kleber et al. 2005; Mikutta et al. 2006, 2009; Rasmussen et al. 2005; Torn et al. 1997). An explanation for the result of uniform reactivity below 25 cm is that stability is predominantly controlled by environmental or physical stabilization mechanisms, not the chemical

structure of organic molecules (Schmidt et al. 2011). The constant  $\mu E$  below the Oa could be analogous to the energy required to disrupt the surface adsorption of the OC where there are sufficient mineral surfaces available.

Experimental adsorption–desorption studies provide a basis for comparison with our data. Generally, these experiments use one organic molecule and a single synthetic mineral, and have found that surface adsorption reactions give bonding energies in the 125–320 kJ mol<sup>-1</sup> range for carboxyl and hydroxyl functional groups on iron oxides (Gu et al. 1995). These experiments yield relative energy ranges broadly similar to what we have found with the RPO analysis, however they are not directly analogous. In the RPO instrument, we are likely measuring the bonding energies of desorption and the oxidation of many different OC compounds. RPO does not give absolute  $E$  values, rather the results are best interpreted as a relative energy distribution of the bonding environment within and locally surrounding the organic molecules. Nevertheless, it is useful to compare the RPO results to other calculated activation energy values with thermal methods (differential scanning calorimetry, DSC). One study of mineral and organic soil horizons using DSC gave a remarkably similar average  $E_a$  value of 136 kJ mol<sup>-1</sup> for all soils measured (Leifeld and von Lutzow 2014). From RPO  $\mu E$  data, we suspect the mobilized DOC is likely adsorbing to mineral surfaces below the Oa horizon where there is plenty of mineral surface relative to OC (Fig. 1). The constant and somewhat lower  $\mu E$  (140 kJ mol<sup>-1</sup>) below the Oa is consistent with a mineral stabilization mechanism as the primary control on soil C stability in the mineral soil. The lower  $\mu E$  values relative to unassociated SOC indicate that the stability of SOC associated with mineral surfaces could be less sensitive to temperature.

#### Relationship between SOC age and reactivity

One of the powerful features of RPO is its ability to probe the relationship among OC bonding environments, source, and age independently. Hawaiian soil samples at Pu‘u Eke (as well as unpublished data from similar sites in Hawaii) run on the RPO system thus far show small variation in the  $F_m$  values between thermal fractions (Fig. 2). For the Oa horizon there was only a 0.79% total change ( $F_m$  range of

1.031–1.015) between fractions. The flat radiocarbon distribution across fractions in the Oa and the single, dominant peak of the  $p(\theta, E)$  are suggestive of a well-mixed, ‘modern’ OC pool in this horizon. For the deeper Bhs and Bg horizons, there was a small systematic decrease in  $F_m$  between F1 and F5, and this change is negatively correlated with computed  $\mu E_f$  of each fraction (Fig. 6). While there is a strong correlation coefficient (respectively  $r^2$  of 0.93 and of 0.98 for the Bhs and Bg horizons) the range in <sup>14</sup>C composition is small when compared to samples of different environments such as sediments, where changes in <sup>14</sup>C age across fractions sometimes exceeds 20,000 years (Hemingway et al. 2017b; Rosenheim and Galy 2012). In addition, in the Pu‘u Eke soils there is no relationship between source ( $\delta^{13}\text{C}$ ) and  $E$  (SI Table S2). In previous RPO studies involving riverine sediments, differences in radiocarbon years between fractions were thousands of years and likely due to mixing of biospheric or petrogenic carbon within river loads and sediments (Hemingway et al. 2017b; Rosenheim and Galy 2012). Sediments have, along with longer OC turnover times, severe O<sub>2</sub> limitation which lead to environments where carbon can undergo chemical differentiation and preservation of reaction products. To achieve persistent OC in relatively well-oxygenated soil, an external stabilization mechanism such as mineral sorption or co-precipitation is essential. Data from the Pu‘u Eke soils, with one dominant peak in the thermogram and relatively consistent  $F_m$  values of the fractions, are consistent with the hypothesis that mineral-organic interactions are a stronger control on  $E$  than either oxygen supply per se or carbon compound composition.

A study of paleosols that used RPO in PY mode did find invariant <sup>14</sup>C ages between fractions (Vetter et al. 2017) and attributed it to the unique properties of paleosols rather than to soils generally. They assumed extremely rapid soil turnover in the Holocene Mississippi Delta that homogenized the <sup>14</sup>C content across the thermochemical spectrum during pedogenesis, and that subsequent burial prevented modern <sup>14</sup>C infiltration into the system, leading to flat  $F_m$  values across the fractions. However, in our soil, at depth, there is small variation in  $F_m$  despite clear evidence of the influx of modern OC into the system. We cannot attribute this finding to carbon burial and isolation from near-surface chemical processes. We propose that it is more indicative of rapid turnover and

decomposition of ‘modern’ OC from the Oa horizon that homogenizes most OC across the thermal gradient because at Pu‘u Eke we see both modern OC along surface coatings at depth and bulk OC with an age of 2500 radiocarbon years, but little radiocarbon differentiation across the different thermal fractions. Within each thermal fraction, there must be a mixture of organic carbon that has the same thermal activation energy and the same average radiocarbon age.

However, the rate of  $^{14}\text{C}$  depletion with increasing activation energy appears to increase with soil depth; the greatest change in age between thermal fractions is in the deepest Bg horizon and is 626 radiocarbon years between  $f_1$  and  $f_5$ . This difference in age between thermal fractions indicates that in deeper soil, OC with the highest  $\mu E_f$  is older than low  $\mu E_f$  OC (Fig. 6). If this pattern results from a mixing of older and younger sources, the younger component has a low  $\mu E_f$ , and the older component has a higher  $\mu E_f$  similar to what we observed in the Oa horizon. As face value this observation is not compatible with the addition of a young component derived from the Oa, but the variation in activation energy may reflect other processes than mixing. Mechanistically, the change in radiocarbon age along the  $E$  continuum can be explained by the competition between the kinetics of sorption/desorption reactions occurring at mineral surfaces and the rate of microbial activity (Rothman and Forney 2007).

## Conclusion

Our study is the first to evaluate the C properties in an active, non-buried, soil profile using the RPO instrument, allowing us to gain a fundamental understanding of how soil OC changes by depth. RPO analysis of Pu‘u Eke samples yielded two main results: (1) constant  $\mu E$  below the Oa horizon even with increasing age and (2) small radiocarbon age increase across the thermal gradient at depth. At Pu‘u Eke, the shallow Oa horizon has a modern radiocarbon value, indicating young inputs, yet has the highest measured RPO  $\mu E$  measured in the soil profile. In previous studies using the RPO modern  $Fm$  values were evolved at the lowest temperatures (i.e. lowest  $E$  values). RPO data for the deeper horizons yields near-constant  $\mu E$  values that are independent of changes in chemistry (e.g. OC content), consistent with mineral stabilization of SOC.

The deeper, mineral-stabilized samples have lower  $\mu E$  than the high-TOC Oa horizon, implying a lower temperature sensitivity for the mineral-stabilized carbon. We show that below the Oa horizon of Pu‘u Eke, the measured  $E$  distribution of OC does not change, even as it ages and the OC concentration decreases.

Our result show that the OC in the Oa horizon at this site has high OC/Ti and a high  $\mu E$ , suggesting that its decomposition is likely strongly temperature-dependent. The radiocarbon age of this material is essentially modern, indicating that it is not stabilized over longer time scales. There is no evidence for an old component in this material, which may reflect the limited mineral matrix available for interaction with carbon compounds. The OC in the deeper Bhs and Bg horizons has lower  $\mu E$ , significantly lower OC/Ti and is considerably older. We propose that these differences reflect greater importance of mineral-OC interactions at depth. Predicting whether OC will persist in the environment relies on a combination of factors, and thermal activation energy adds an important insight into OC stability. The dominance of carbon molecular structure as the main predictor for persistence has been challenged (Hemingway et al. 2019; Lehmann and Kleber 2015; Schmidt et al. 2011), but the idea that as soil carbon ages it becomes harder to decompose is still widespread in the literature. There is however a growing understanding that the rate of C mineralization in soils is a strong function of the soil environment and mineral-carbon interactions (Schmidt et al. 2011). The RPO approach allows us to directly test this hypothesis.

RPO is a powerful tool to probe the relationship between the thermal reactivity,  $\delta^{13}\text{C}$ , and radiocarbon. This study provided an initial, detailed analysis of the RPO technique on a small set of well-studied soils. We were able to leverage the existing understanding of this soil environment to propose some working hypotheses for the RPO results in these soils. We show the RPO instrument can detect energetic differences in organic and mineral horizons. This study lays the foundation to utilize RPO to understand mineral-organic carbon stabilizing interactions across a wide range of soil environments.

**Acknowledgements** We would like to thank the staff at NOSAMS for their generous laboratory help and guidance, especially A. Mchnicol, M. Lardie Gaylord, and A. Gagnon. K. Grant would like to thank J. Hemingway for his assistance with the RPO instrument and help with the ‘rampedpyrox’ code,

and Gregg McElwee for assistance with ICP instrumentation at Cornell. Marc Kramer helped with field sampling and interpretation of soil organic C properties in the soil horizon.

**Funding** This work was partially supported by the Cornell University Atkinson Center Small Grant program and by NSF EAR 1660923 (Derry, PI). KEG was supported by the Cross-Scale Biogeochemistry and Climate – National Science Foundation Integrative Graduate Education and Research Traineeship grant#DGE-1069193 and the Cornell Graduate Fellowship.

## References

- Barre P, Plante AF, Cecillon L, Lutfalla S, Baudin F, Bernard S, Christensen BT, Eglin T, Fernandez JM, Houot S, Katterer T, Le Guillou C, Macdonald A, van Oort F, Chenu C (2016) The energetic and chemical signatures of persistent soil organic matter. *Biogeochemistry* 130(1–2):1–12
- Bianchi TS, Galy V, Rosenheim BE, Shields M, Cui XQ, Van Metre P (2015) Paleoreconstruction of organic carbon inputs to an oxbow lake in the Mississippi River watershed: effects of dam construction and land use change on regional inputs. *Geophys Res Lett* 42(19):7983–7991
- Bradford MA, Wieder WR, Bonan GB, Fierer N, Raymond PA, Crowther TW (2016) Managing uncertainty in soil carbon feedbacks to climate change. *Nat Clim Change* 6(8):751–758
- Buettner SW, Kramer MG, Chadwick OA, Thompson A (2014) Mobilization of colloidal carbon during iron reduction in basaltic soils. *Geoderma* 221–222:139–145
- Chadwick OA, Gavenda RT, Kelly EF, Ziegler K, Olson CG, Elliott WC, Hendricks DM (2003) The impact of climate on the biogeochemical functioning of volcanic soils. *Chem Geol* 202(3–4):195–223
- Chadwick OA, Kelly EF, Hotchkiss SC, Vitousek PM (2007) Precontact vegetation and soil nutrient status in the shadow of Kohala Volcano, Hawaii. *Geomorphology* 89(1–2):70–83
- Chorover J, Amistadi MK, Chadwick OA (2004) Surface charge evolution of mineral-organic complexes during pedogenesis in Hawaiian basalt. *Geochim Cosmochim Acta* 68:4859–4876
- Davidson EA, Janssens IA (2006) Temperature sensitivity of soil carbon decomposition and feedbacks to climate change. *Nature* 440(7081):165–173
- Feng WT, Plante AF, Six J (2013a) Improving estimates of maximal organic carbon stabilization by fine soil particles. *Biogeochemistry* 112(1–3):81–93
- Feng X, Vonk JE, Van Dongen BE, Gustafsson Ö, Semiletov IP, Dudarev OV, Wang Z, Montluçon DB, Wacker L, Eglinton TI (2013b) Differential mobilization of terrestrial carbon pools in Eurasian Arctic river basins. *Proc Natl Acad Sci USA* 110(35):14168–14173
- Giambelluca TW, Nullet MA, Schroeder TA (1986) Rainfall atlas of Hawai'i. Department of Land and Natural Resources, Hawai'i
- Giambelluca TW, Chen Q, Frazier AG, Price JP, Chen Y-L, Chu PS, Eischeid K, Delparte DM (2013) Online rainfall atlas of Hawai'i. *Bull Am Meteorol Soc* 94:313–316
- Gu BH, Schmitt J, Chen Z, Liang LY, McCarthy JF (1995) Adsorption and desorption of different organic-matter fractions on iron-oxide. *Geochim Cosmochim Acta* 59(2):219–229
- Hemingway JD (2016) rampedpyrox: open-source tools for thermoanalytical data analysis. <http://pypi.python.org/pypi/rampedpyrox>. Accessed 5 Aug 2018
- Hemingway JD, Galy VV, Gagnon AR, Grant KE, Rosengard SZ, Soulet G, Ziegler PK, McNichol AP (2017a) Assessing the blank carbon contribution, isotope mass balance, and kinetic isotope fractionation of the ramped pyrolysis/oxidation instrument at NOSAMS. *Radiocarbon* 59(1):179–193
- Hemingway JD, Rothman DH, Rosengard SZ (2017b) Galy VV (2017b) Technical note: an inverse method to relate organic carbon reactivity to isotope composition from serial oxidation. *Biogeosciences* 14:5099–5114
- Hemingway JD, Hilton RG, Hovius N, Eglinton TI, Haghpor N, Wacker L, Chen M-C, Galy VV (2018) Microbial oxidation of lithospheric organic carbon in rapidly eroding tropical mountain soils. *Science* 360(6385):209–212
- Hemingway JD, Rothman DH, Grant KE, Rosengard SZ, Eglinton TI, Derry LA, Galy VV (2019) Mineral protection regulates the global preservation of natural organic carbon. *Nature* 570(7760):228
- Jackson RB, Lajtha K, Crow SE, Hugelius G, Kramer MG, Pineiro G (2017) The ecology of soil carbon: pools, vulnerabilities, and biotic and abiotic controls. *Annu Rev Ecol Evol Syst* 48(48):419–445
- Kaiser K, Guggenberger G (2003) Mineral surfaces and soil organic matter. *Eur J Soil Sci* 54(2):219–236
- Kleber M, Mikutta R, Torn, Jahn R (2005) Poorly crystalline mineral phases protect organic matter in acid subsoil horizons. *Eur J Soil Sci* 56(6):717–725
- Kramer MG, Sanderman J, Chadwick OA, Chorover J, Vitousek PM (2012) Long-term carbon storage through retention of dissolved aromatic acids by reactive particles in soil. *Glob Change Biol* 18(8):2594–2605
- Kurtz AC, Derry LA, Chadwick OA, Alfano MJ (2000) Refractory element mobility in volcanic soils. *Geology* 28(8):683–686
- Kurtz AC, Derry LA, Chadwick OA (2001) Accretion of Asian dust to Hawaiian soils: isotopic, elemental, and mineral mass balance. *Geochim et Cosmochim Acta* 65:1971–1983
- Lehmann J, Kleber M (2015) The contentious nature of soil organic matter. *Nature* 528(7580):60–68
- Leifeld J, von Lutzow M (2014) Chemical and microbial activation energies of soil organic matter decomposition. *Biol Fertil Soils* 50(1):147–153
- Lopez-Capel E, Krull ES, Bol R, Manning DAC (2008) Influence of recent vegetation on labile and recalcitrant carbon soil pools in central Queensland, Australia: evidence from thermal analysis-quadrupole mass spectrometry-isotope ratio mass spectrometry. *Rapid Commun Mass Spectrom* 22(11):1751–1758
- Marin-Spiotta E, Chadwick OA, Kramer M, Carbone (2011) Carbon delivery to deep mineral horizons in Hawaiian rain

- forest soils. *J. Geophys. Res.* <https://doi.org/10.1029/2010JG001587>
- Marín-Spiotta E, Gruley KE, Crawford J, Atkinson EE, Miesel JR, Greene S, Cardona-Correa C, Spencer RGM (2014) Paradigm shifts in soil organic matter research affect interpretations of aquatic carbon cycling: transcending disciplinary and ecosystem boundaries. *Biogeochemistry* 117(2–3):279–297
- McNichol AP, Osborne EA, Gagnon AR, Fry B, Jones GA (1994) TIC, TOC, DIC, DOC, PIC, POC—unique aspects in the preparation of oceanographic samples for C-14 AMS. *Nucl Instrum Methods Phys Res Sect B* 92(1–4):162–165
- Mikutta R, Kleber M, Torn MS, Jahn R (2006) Stabilization of soil organic matter: association with minerals or chemical recalcitrance? *Biogeochemistry* 77(1):25–56
- Mikutta R, Schaumann GE, Gildemeister D, Bonneville S, Bonneville S, Kramer MG, Chorover J, Chadwick OA, Guggenberger G (2009) Biogeochemistry of mineral-organic associations across a long-term mineralogical soil gradient (0.3–4100 kyr), Hawaiian Islands. *Geochim et Cosmochim Acta* 73(7):2034–2060
- Ohno T, Heckman KA, Plante AF, Fernandez IJ, Parr TB (2017) 14 C mean residence time and its relationship with thermal stability and molecular composition of soil organic matter: a case study of deciduous and coniferous forest types. *Geoderma* 308:1–8
- Plante AF, Fernandez JM, Leifeld J (2009) Application of thermal analysis techniques in soil science. *Geoderma* 153(1–2):1–10
- Plante AF, Beupre SR, Roberts ML, Baisden T (2013) Distribution of radiocarbon ages in soil organic matter by thermal fractionation. *Radiocarbon* 55(2–3):1077–1083
- Rasmussen C, Torn MS, Southard RJ (2005) Mineral assemblage and aggregates control carbon dynamics in a California Conifer forest. *Soil Sci Soc Am J* 69(6):1711
- Rosenheim BE, Galy V (2012) Direct measurement of riverine particulate organic carbon age structure. *Geophys Res Lett.* <https://doi.org/10.1029/2012GL052883>
- Rosenheim BE, Day MB, Domack E, Schrum H, Benthien A, Hayes JM (2008) Antarctic sediment chronology by programmed-temperature pyrolysis: methodology and data treatment. *Geochem, Geophys, Geosyst.* <https://doi.org/10.1029/2007GC001816>
- Rothman DH, Forney DC (2007) Physical model for the decay and preservation of marine organic carbon. *Science* 316(5829):1325–1328
- Schmidt MW, Torn MS, Abiven S, Dittmar T, Guggenberger G, Janssens IA, Kleber M, Kogel-Knabner I, Lehmann J, Manning DA, Nannipieri P, Rasse DP, Weiner S, Trumbore SE (2011) Persistence of soil organic matter as an ecosystem property. *Nature* 478(7367):49–56
- Schreiner KM, Bianchi TS, Rosenheim BE (2014) Evidence for permafrost thaw and transport from an Alaskan North Slope watershed. *Geophys Res Lett* 41(9):3117–3126
- Soulet G, Skinner LC, Beupre SR, Galy V (2016) A note on reporting of reservoir C-14 disequilibria and age offsets. *Radiocarbon* 58(1):205–211
- Thompson A, Chadwick OA, Boman S, Chorover J (2006a) Colloid mobilization during soil iron redox oscillations. *Environ Sci Technol* 40(18):5743–5749
- Thompson A, Chadwick OA, Rancourt DG, Chorover J (2006b) Iron-oxide crystallinity increases during soil redox oscillations. *Geochim Cosmochim Acta* 70(7):1710–1727
- Torn MS, Trumbore SE, Chadwick OA, Vitousek PM, Hendricks DM (1997) Mineral control of soil organic carbon storage and turnover. *Nature* 389(6647):170–173
- Trumbore S (2009) Radiocarbon and soil carbon dynamics. *Annu Rev Earth Planet Sci* 37:47–66
- Vetter L, Rosenheim BE, Fernandez A, Tornqvist TE (2017) Short organic carbon turnover time and narrow C-14 age spectra in early Holocene wetland paleosols. *Geochem Geophys Geosyst* 18(1):142–155
- Williams EK, Rosenheim BE (2015) What happens to soil organic carbon as coastal marsh ecosystems change in response to increasing salinity? an exploration using ramped pyrolysis. *Geochem Geophys Geosyst* 16(7):2322–2335
- Williams EK, Rosenheim BE, McNichol AP, Masiello CA (2014) Charring and non-additive chemical reactions during ramped pyrolysis: applications to the characterization of sedimentary and soil organic material. *Org Geochem* 77:106–114
- Williams EK, Fogel ML, Berhe AA, Plante AF (2018) Distinct bioenergetic signatures in particulate versus mineral-associated soil organic matter. *Geoderma* 330:107–116. <https://doi.org/10.1016/j.geoderma.2018.05.02>
- Zhang XW, Bianchi TS, Cui XQ, Rosenheim BE, Ping CL, Hanna AJM, Kanevskiy M, Schreiner KM, Allison MA (2017) Permafrost organic carbon mobilization from the watershed to the Colville River delta: evidence from C-14 ramped pyrolysis and lignin biomarkers. *Geophys Res Lett* 44(22):11491–11500

**Publisher's Note** Springer Nature remains neutral with regard to jurisdictional claims in published maps and institutional affiliations.